Physical Properties of Summer Sea Ice in the Pacific Sector of the Arctic During 2008–2018

Article *in* Journal of Geophysical Research: Oceans · September 2020

DOI: 10.1029/2020JC016371

6 authors, including:

Qingkai Wang
Dalian University of Technology
22 PUBLICATIONS **133** CITATIONS
SEE PROFILE

Bin Cheng
Finnish Meteorological Institute
133 PUBLICATIONS **2,307** CITATIONS
SEE PROFILE

Zhijun Li
Dalian University of Technology
193 PUBLICATIONS **1,611** CITATIONS
SEE PROFILE

JGR Oceans

RESEARCH ARTICLE
10.1029/2020JC016371

Physical Properties of Summer Sea Ice in the Pacific Sector of the Arctic During 2008–2018

Q. Wang[1,2], P. Lu[1], M. Leppäranta[3], B. Cheng[4], G. Zhang[2], and Z. Li[1]

[1]State Key Laboratory of Coastal and Offshore Engineering, Dalian University of Technology, Dalian, China, [2]School of Naval Architecture Engineering, Dalian University of Technology, Dalian, China, [3]Institute of Atmospheric and Earth Sciences, University of Helsinki, Helsinki, Finland, [4]Finnish Meteorological Institute, Helsinki, Finland

Key Points:
- New parameterizations of salinity and density for late summer first-year ice (FYI) and multiyear ice (MYI) are proposed
- Mean bulk brine and gas volume fractions are 11.3 ± 6.2% and 14.9 ± 7.9% for FYI and 9.5 ± 11.0% and 13.5 ± 12.7% for MYI in late summer
- The energy used to melt a unit volume of sea ice is $(2.26 \pm 0.29) \times 10^5$ kJ for FYI and $(2.36 \pm 0.24) \times 10^5$ kJ for MYI in late summer

Correspondence to:
Z. Li,
lizhijun@dlut.edu.cn

Citation:
Wang, Q., Lu, P., Leppäranta, M., Cheng, B., Zhang, G., & Li, Z. (2020). Physical properties of summer sea ice in the Pacific sector of the Arctic during 2008–2018. *Journal of Geophysical Research: Oceans*, *125*, e2020JC016371. https://doi.org/10.1029/2020JC016371

Received 4 MAY 2020
Accepted 24 AUG 2020
Accepted article online 26 AUG 2020

Abstract Sea ice physical properties were determined at 21 first-year ice (FYI) and 20 multiyear ice (MYI) stations in the Pacific sector of the Arctic during summer in 2008–2018. The bulk ice temperature was between −2.7 and −0.3 °C for FYI and between −1.7 and −0.2 °C for MYI. The bulk salinity was 0.4–3.2 practical salinity unit (psu) for FYI and 0.4–2.4 psu for MYI. A low-salinity layer and an almost fresh layer were always present at the top of FYI and MYI, respectively. The bulk density was 600.3–900.1 kg/m^3 for FYI and 686.1–903.3 kg/m^3 for MYI. The upper layer density was less than the lower layer density due to higher gas content. Salinity and density were less than previously reported values of summer sea ice, and their parameterization formulae were updated. The brine and gas volume fractions were determined based on the measured ice temperature, salinity, and density. The average bulk brine and gas volume fractions were 11.3 ± 6.2% and 14.9 ± 7.9% for FYI and 9.5 ± 11.0% and 13.5 ± 12.7% for MYI. Typical brine and gas volume fraction profiles were identified and parameterized using regression analysis. The large brine and gas content of sea ice affects the sea ice melting. The energy used to melt a unit volume of summer Arctic sea ice was estimated as $(2.26 \pm 0.29) \times 10^5$ kJ for FYI and $(2.36 \pm 0.24) \times 10^5$ kJ for MYI. This study shows that the current physical state of the Arctic summer sea ice is different from earlier sea ice climatology, and the results will guide further research and modeling of Arctic sea ice.

Plain Language Summary Arctic sea ice has undergone dramatic changes during the recent decades. Both ice thickness and extent have declined. However, it has remained unclear whether sea ice physical properties, such as temperature, salinity, and density, have changed in response to the Arctic warming. In this study, we present an analysis of measurements of sea ice physical properties in the late summer over the past 10 years in the Pacific sector of the Arctic Ocean. We found that the salinity and density of summer Arctic sea ice were lower than in earlier studies, and thus, their previous parameterizations need to be updated, and therefore, new parameterizations are proposed here. With the enhanced melt of the summer Arctic sea ice, the fractions of the sea ice phase components (pure ice, brine, and gas) have changed. The vertical profiles of the brine and gas volume fractions with depth are also quantified for future research and modeling efforts. The findings will help to improve the accuracy of existing sea ice models.

1. Introduction

Sea ice is known to have important impacts on the climate (Arctic Monitoring and Assessment Programme, 2011; Vihma, 2014), ecosystem (Meier et al., 2014), and marine activities (Arctic Council, 2009; Smith & Stephenson, 2003) in the Arctic. The fundamental physical properties of sea ice, including temperature, salinity, and density, play a key role in the evolution of the Arctic sea ice cover. These properties affect, for example, the surface albedo (Perovich & Grenfell, 1981), primary production (Gosselin et al., 1997), and the mechanical and thermal properties of sea ice (Timco & Weeks, 2010).

Sea ice temperature, salinity, and density can be measured directly in the field. The annual cycle of Arctic sea ice temperature has been investigated using thermistor strings (Perovich & Elder, 2001). The general seasonal evolution of ice temperature is as follows: sea ice becomes cold and begins to grow in the late fall when a cold front accompanying with a low-pressure system propagates through the ice

and then warms to the melting stage in the following summer. Vertical temperature profiles of Arctic sea ice have also been measured from ice cores in the International Polar Year Circumpolar Flaw Lead system study, and several profile types were identified related to different atmospheric conditions (Carnat et al., 2013).

Previous studies on sea ice salinity have shown that first-year ice (FYI) usually exhibits a "C-shaped" vertical profile during growth (Nakawo & Sinha, 1981) and turns to a "?-shape" in the melt season (Tucker et al., 1987). Multiyear ice (MYI) is less saline than FYI due to desalination in the previous seasons and always has a nearly fresh surface layer (Tucker et al., 1987). General relationships have been found between ice thickness and bulk salinity, which differ for sea ice in the growth (Cox & Weeks, 1974) and melt (Eicken et al., 1995; Overgaard et al., 1983; Tucker et al., 1987) seasons. The two main mechanisms causing salt loss from sea ice in winter and summer are brine gravity drainage and flushing by surface melting (Notz & Worster, 2009). Brine advection depends on the permeability of sea ice, and columnar-grained ice is effectively permeable when the brine volume fraction exceeds 5% (Golden et al., 1998).

Measurements of sea ice density can be found in several studies (e.g., Forsström et al., 2011; Frantz et al., 2019; Ukita et al., 2000). There are four different techniques to measure sea ice density including mass/volume, displacement (submersion), specific gravity, and freeboard and ice thickness methods (Timco & Frederking, 1996). For a core-based ice density measurement, such as the mass/volume method, brine drainage and measurement errors of mass and dimensions are two major sources of uncertainty. The underestimation caused by brine drainage might be at least 5% (Hutchings et al., 2015), and the uncertainty due to the volume measurement error depends on the size of the ice sample and can be estimated through error propagation (Hutchings et al., 2015; Pustogvar & Kulyakhtin, 2016). Eicken et al. (1995) parameterized the vertical density profile of Arctic sea ice density using a logarithmic equation based on the measurements from 14 MYI cores in late summer. Typically, sea ice density is lower above the water surface level than below it in summer due to air-filled pores originating from the freeboard melting process. To the authors' best knowledge, there have been only a few studies on the vertical profile of the brine volume fraction within Arctic sea ice (Carnat et al., 2013; Eicken et al., 1995; Overgaard et al., 1983; Perovich & Gow, 1996) and even less on the profile of the gas volume fraction (Eicken et al., 1995; Nakawo, 1983). Eicken et al. (1995) reported that for the summer MYI in the Atlantic sector of the Arctic (ASA), the brine volume fraction ranged from 8% to 15% and the gas volume fraction decreased from >20% at the top to <5% below 1 m depth. Carnat et al. (2013) plotted the temporal evolution of the vertical brine volume fraction profiles in the Canadian Arctic and compared them to the permeability threshold. The results showed that the brine volume fraction and permeability varied with ice temperature during the growth cycle.

Large variations in Arctic sea ice conditions, such as the consistent reduction in ice volume (Gascard et al., 2019) and thickness (Lindsay & Schweiger, 2015), have been observed because of the Arctic amplification in recent decades (Screen & Simmonds, 2010). The physical characteristics of sea ice are likely to change with the Arctic warming. With increased air temperature, the sea ice melt season has lengthened in recent summers (Markus et al., 2009). The melt of highly reflective snow and ice lowers the surface albedo that results in stronger absorption of solar energy by the upper ocean leading to enhanced warming (Arctic Monitoring and Assessment Programme, 2011; Riihelä et al., 2013). As a result, the multiphase structure of sea ice is expected to change accordingly that further affects other sea ice physical properties (Hunke et al., 2011; Light et al., 2004). Some of the parameterization formulae for sea ice physical properties in mathematical models are still based on earlier observations and may be inaccurate, possibly introducing error sources to modeling results. Therefore, the knowledge on the physical properties of summer Arctic sea ice needs to be updated. However, to our knowledge, high-quality measurements of sea ice physical properties have been sparse since the year 2000.

In this study, we present in situ measurements of the fundamental physical properties of sea ice from the Pacific sector of the Arctic Ocean (PSA) in the past 10 years. The data were collected by the Chinese National Arctic Research Expedition (CHINARE) program. The motivation of the study was to identify the changes in the state summer sea ice in the PSA. The field data include sea ice temperature, salinity, density, and crystal structure. Using these observations, the brine and gas content of sea ice were first determined, followed by the estimation of energy needed for melting of the sea ice. Finally, a brief interannual

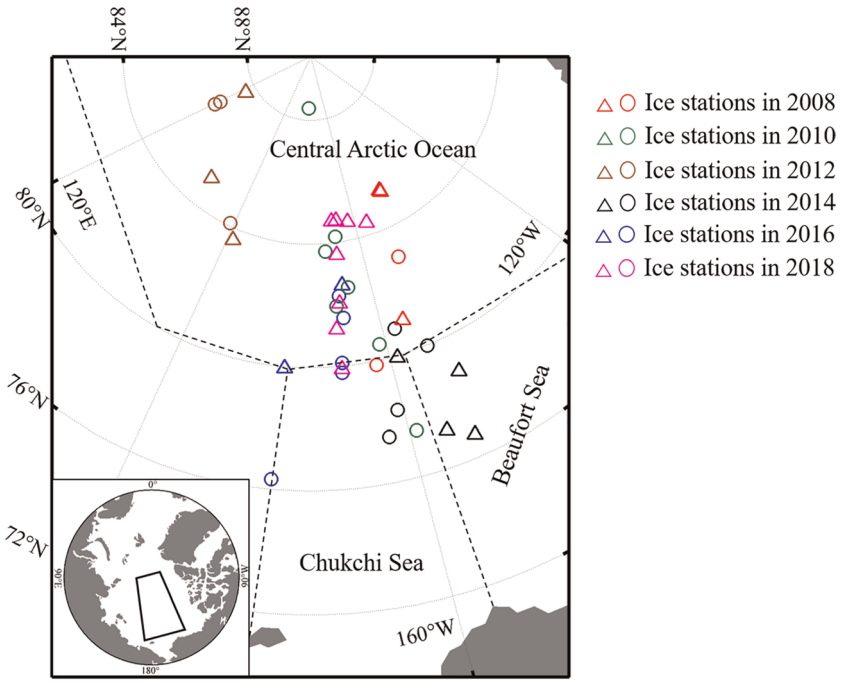

Figure 1. Map of ice stations. The area circled by solid lines in the subplot represents the general location of ice stations in the Arctic Ocean. The regions defined by dashed lines show the Chukchi Sea, Beaufort Sea, and the Central Arctic Ocean based on the division by the National Snow and Ice Data Center. Ice types are also labeled using circles and triangles for FYI and MYI, respectively.

analysis of the physical properties of sea ice was performed. The results provide the physical properties of sea ice in the present Arctic summer to be used for model parameterizations. Mathematical formulae reported in the earlier literature were updated for their parameters based on our new observations. These updated formulae can be utilized in future sea ice research and modeling.

2. Field Sampling and Measurements

CHINARE expeditions have been conducted mostly in the PSA via the Bering Strait (Huang et al., 2013, 2016; Wang et al., 2018) (Figure 1). Ice stations were selected along the cruise routes for ice sampling and detailed field studies. The sites were located on vast ice floes with diameters of several kilometers. A total of 41 ice stations was included during the summers of 2008–2018. The detailed information of the ice stations is listed in Appendix A. Most of the stations were located within the area 76.3–88.4°N and 147.1–179.6°W, except that 2012 stations were located further west, in 83.4–87.4°N and 120.2–161.4°E. According to the division of the Arctic Ocean by the National Snow and Ice Data Center (https://nsidc.org/data/masie/browse_regions), the ice stations were located in the Central Arctic Ocean, except some stations in the Chukchi and Beaufort seas (Figure 1). The ice sampling was carried out mainly in August, except between late August and early September in 2008 and 2012. The Arctic sea ice melt data issued by National Aeronautics and Space Administration's Goddard Earth Science Laboratories (https://earth.gsfc.nasa.gov/cryo/data/arctic-sea-ice-melt) show that the dates of melt onset in PSA in 2010 and 2018 (late June) were approximately 10 days later than in our other investigation years (early June). So our ice cores had experienced at least 1-month melt at the time of sampling. The air temperature ranged between −4.2 and 3.6 °C with an average of −0.6 ± 1.7 °C at the samplings; the minimum occurred in 2008 because the sampling was conducted in the end of the melt season. The sampling sites were selected from wide, smooth areas tens of meters away from melt ponds and floe edge. Each time at least four ice cores were extracted through the floe thickness using a 9-cm-diameter drilling auger for sea ice temperature, salinity, density, and crystal structure measurements. The distances between ice cores were less than 0.2 m to limit spatial variability. Ice thickness ranged from 49.3 to

205.3 cm with an average of 117.5 ± 37.9 cm for FYI and from 104.7 to 183.3 cm with an average of 138.0 ± 24.9 cm for MYI. These values are similar with the thickness at the summer sampling sites reported in Carnat et al. (2013), Frantz et al. (2019), and Overgaard et al. (1983). Our ice thickness values can be considered representative as they compare well with the mean ice thickness along summer cruise tracks in the PSA in Perovich et al. (2009) and Tucker et al. (1999), where ice thickness was estimated by scaling overturned ice blocks along ship's hull with a calibrated measure near the waterline. In almost all cores, layers with massive gas inclusions and low structural integrity were present at the surface. Large cavities showed up below the surface because of meltwater penetration, indicating that sea ice in the top layer had experienced a severe surface ablation. Some cavities appeared near the ice bottom in the skeleton layer due to brine drainage. The range of snow thickness was 3–20 cm with a mean value of 8.6 ± 4.1 cm. Generally, there was a thin fresh snow layer underlain by a coarse-grained snow layer, which had metamorphosed from fresh snow by sintering and melt-freeze cycles.

The sea ice temperature was measured at each site immediately after lifting the ice core using a fast-response probe thermometer (accuracy ±0.2 °C, Testo, Germany). The probe was inserted in 2-mm diameter holes drilled to the core center at 5- to 10-cm intervals along the core length. Another core was then extracted and cut into 5–10 cm long segments using a stainless steel saw. To minimize the brine drainage, we cut the cores immediately after removal and placed the core sections into sealed plastic containers. The salinity samples were melted aboard the ship, and a salinometer with an accuracy of 0.1 practical salinity unit (psu) was used to measure the salinity at a room temperature.

The salinity obtained by a core-based measurement is always less than the actual in situ value because of the loss of brine from the extracted core, particularly in the warm and high-salinity sections. To reduce the measurement error, rapid processing of cores on site is required (Carnat et al., 2013; Eicken et al., 2014). A quantitative estimation of the error of core-based salinity measurement is not easy. This method has been adopted in many studies (e.g., Carnat et al., 2013; Frantz et al., 2019; Tucker et al., 1999), while only a few studies have reported the measurement error. Comparing with nondestructive measurements, Notz et al. (2005) found that using core measurements the salinity underestimation in the bottom sea ice layer ranged from 1 to 20 psu for growing sea ice. Eicken et al. (1995) concluded that the measured salinities of summer MYI may be artificially shifted down only by a few tenths on average, but it is the main contributor to the scatter in the data.

The other two ice cores were placed in whole length into sealed plastic containers and stored in a cold laboratory aboard the ship at an ambient temperature of −18 °C. One core was prepared for density measurements in a cold laboratory with temperature below −10 °C using the mass/volume method (Timco & Frederking, 1996). Therefore, melting of samples or brine loss during the preparation was not expected (Pustogvar & Kulyakhtin, 2016). The core was first cut along the core length into 5–10 cm long sections, which were then machined into cubes with sides of 4 cm using a band saw to avoid errors due to surface irregularities caused by core drilling. The mass of the cube was weighed using a balance (±0.1 g), and the volume was calculated based on the dimensions measured using a caliper (±0.02 mm). The uncertainty of the estimated sea ice density can be attributed to two main sources: measurement error and brine loss during the core sampling. The uncertainty caused by measurement error can be evaluated with an error propagation analysis (Hutchings et al., 2015; Pustogvar & Kulyakhtin, 2016). Here, the accuracy of dimension measurement was assumed as ±1 mm, although the caliper had an original accuracy of ±0.02 mm, since the summer sea ice could not be incised precisely. An ice cube typically had a mass of 40–70 g, and thus, the uncertainty due to the measurement error was approximately 5%. To quantify the underestimation due to brine drainage is not easy. Hutchings et al. (2015) pointed out that the brine drainage might cause mass/volume density estimates to be at least 5% too low, even though care is taken to move cores quickly to a freezer. Pustogvar and Kulyakhtin (2016) further evaluated the upper limit of the uncertainty due to the brine drainage on mass/volume method as 20%.

The last ice core was stored for ice crystal structure measurements by first preparing 1 cm thick vertical sections 5–10 cm in length using a band saw. These thick sections were attached to glass plates and cut further to an approximately 2 mm thickness. A microtome was then used to reduce the thickness to 0.5 mm. These thin sections were placed on a universal stage to observe the crystal structure under crossed polarized light, recorded by photography.

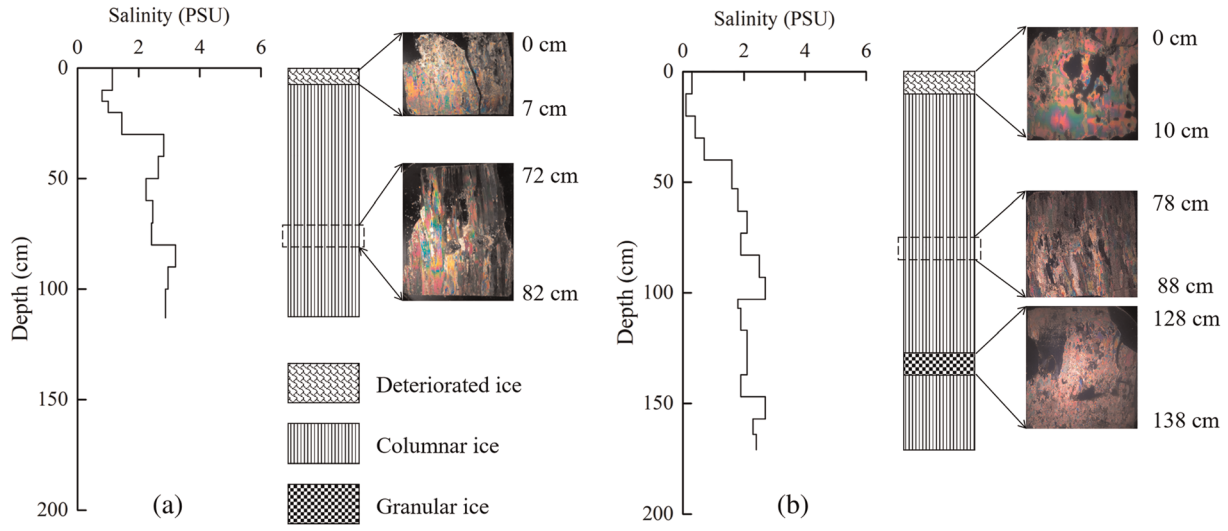

Figure 2. Examples of the salinity-crystal structure profiles for (a) FYI at 12S1 and (b) MYI at 14S1. The salinity in the upper layer of FYI is slightly higher than that in MYI. The FYI sample consists of 93% columnar ice overlain by 7% deteriorated ice. The MYI sample shows a granular ice layer between two columnar ice layers.

3. Results

The ice stations were classified into FYI and MYI types based on the salinity profile and crystal texture. The salinity profile is commonly used to distinguish between FYI and MYI, especially when the thickness and ice surface morphology may indicate otherwise. In general, a MYI salinity profile shows a fresh top layer in the ice sheet due to desalinization during the previous seasons (Vancoppenolle et al., 2006). However, surface melting may also lower the salinity in the FYI top layer, which makes the distinction between FYI and MYI profiles subtle. Thus, auxiliary information from the ice crystal structure is necessary because MYI always shows discontinuities in crystal structure related to the changes in the size and shape of crystals (Tucker et al., 1987). Applying these criteria, 21 FYI stations and 20 MYI stations were identified. Representative examples of FYI and MYI salinity-crystal structure profiles are shown in Figure 2.

3.1. Sea Ice Crystal Structure

The results of the ice crystal structure measurements conducted during 2012–2018 are presented here. Columnar, granular, and deteriorated ice were identified in most of the cores. Columnar grains were well-ordered vertical columns (Figure 3a), usually formed as the result of congelation under quiescent growth conditions (Eicken & Lange, 1989). Columnar congelation ice accounted for on average 85 ± 12% and 66 ± 30% of the ice thickness in FYI and MYI, respectively.

Granular ice (Figure 3b) accounted for 3 ± 7% of the FYI thickness and 16 ± 19% of the MYI thickness. Granular ice mainly appeared in the middle of a core, which is opposite to previous studies where the granular ice was usually in the upper ice layers (Carnat et al., 2013; Perovich et al., 2009; Tucker et al., 1999). A possible cause is internal melting and recrystallization. In addition, open leads and melt ponds developed in summer likely produce frazil ice in the early growing season. The frazil may move to form granular layers underneath existing floes by drifting in turbulent flows or by rafting after consolidation (Lange & Eicken, 1991).

In our observations, the ice in the top layer was highly porous and deteriorated to a great degree. The crystals resembled granular texture but were retextured without clear boundaries and could not be accurately classified (Figure 3c). In combination with the low density in the upper part of an ice core (see section below), this layer can be considered as deteriorated superimposed ice or snow ice, which had formed by snow-to-ice transformation (Cheng et al., 2003). The snow-to-ice transformation accounted on average for 11 ± 8% and

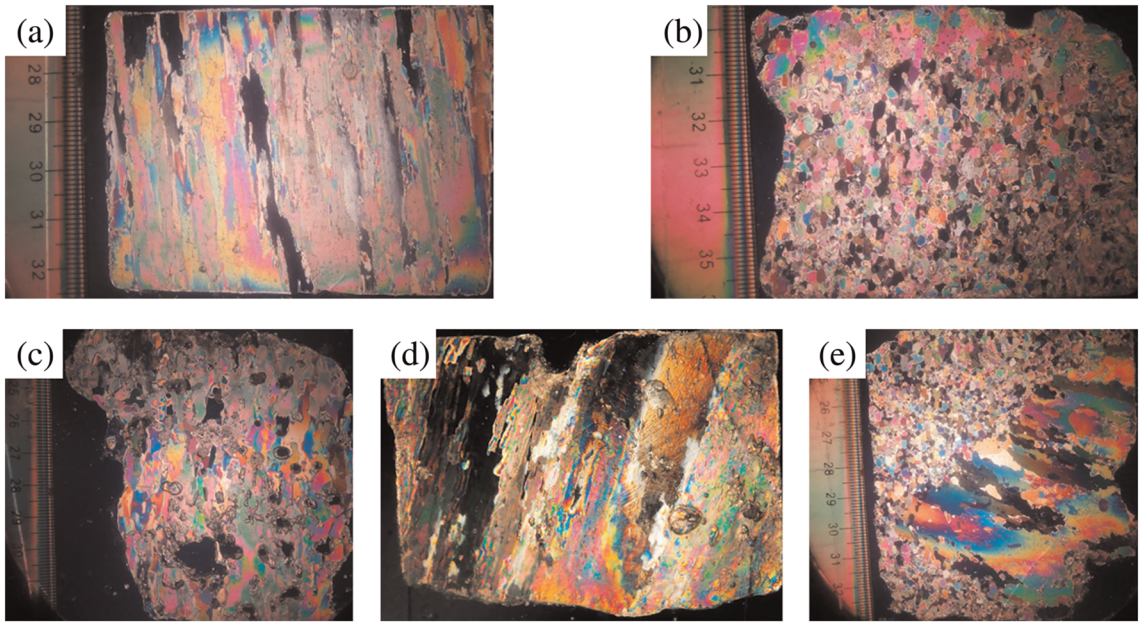

Figure 3. Representative pictures of sea ice crystal structure types: (a) columnar, (b) granular, (c) deteriorated, (d) inclined columnar, and (e) mixed granular/columnar ice.

$10 \pm 12\%$ of the ice thickness in FYI and MYI, respectively, but these numbers may be overestimates due to a major ice deterioration caused by surface melting. Snow-to-ice transformation has been considered as a common process in the Antarctic (Jeffries et al., 2001) but not widespread in the Arctic (Sturm & Massom, 2010). However, due to the thinning of Arctic sea ice and the projected increase in the total annual precipitation, the potential for snow-to-ice transformation will increase (Granskog et al., 2017; Vihma et al., 2014). Snow ice formation has a strong regional variability in the Arctic, and the largest potential is found in the ASA (Merkouriadi et al., 2020). Granskog et al. (2017) found that the contribution of snow ice layers (without superimposed ice) to total ice thickness ranged from 6% to 28% with a mean of 20% in the north of Svalbard in 2015.

Other crystal structure types were classified as inclined columnar ice, when crystals were inclined at a large angle with respect to the vertical (Figure 3d) due to deformation and mixed granular/columnar ice (Figure 3e), when crystals were formed by deformation or represented the transition from granular to columnar congelation ice.

Table 1
Comparison of the Observed Mean Fractions of Sea Ice Crystal Structure Types With Earlier Observations in the PSA

Year	Reference	f_C (%)	f_G (%)	f_O (%)	Sea area	Duration
2005	Perovich et al. (2009)	9	55	36	Chukchi Sea	August–September
		56	39	5	Central Arctic	
1994	Tucker et al. (1999)	93	2	5	Chukchi Sea	July–August
		85	7	8	Central Arctic	
1986–1987	Meese (1989)	92	8		Beaufort Sea	April–May
2007–2008	Carnat et al. (2013)	87	9	4	Beaufort Sea	November–June
		81	6	13	Beaufort Sea	August
2012–2018	This study	78	13	9	Chukchi Sea	
		72	11	17	Central Arctic	

Note. f_C, f_G, and f_O are the mean fractions of columnar, granular, and other structure types.

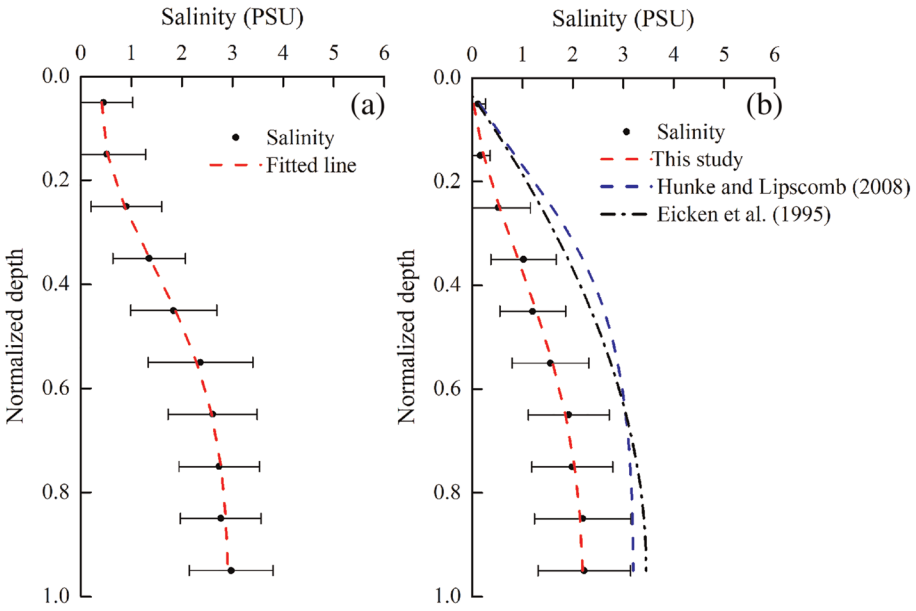

Figure 4. Mean sea ice salinity against normalized depth for (a) FYI and (b) MYI during the melt season. The red dashed lines represent the fit based on the measured data in this study. The error bars represent the standard deviations. The blue dashed line and black dash-dotted line are the MYI profiles derived from Hunke and Lipscomb (2008) and Eicken et al. (1995), respectively.

The mean fractions of columnar, granular, and other (deteriorated, inclined columnar, and mixed granular/columnar crystals) crystal structure types are listed in Table 1. Compared with several earlier studies, our observation of the granular ice fraction is similar to Carnat et al. (2013) and Meese (1989) (nearly 10%) and slightly higher than Tucker et al. (1999). However, the mean granular ice fraction was much higher in Perovich et al. (2009), over 40%. Granular texture is often associated with the formation of frazil ice in turbulent open water conditions. A possible explanation proposed by Perovich et al. (2009) was that their increased granular ice fraction indicated a shift toward greater amounts of frazil ice growth due to increased summer opening and seasonal ice area in the Arctic Ocean, while our result does not support this expectation, warranting for future study. Additionally, it is noteworthy that our mean fraction of granular ice was potentially underestimated since the texture in the surface layer was classified into deteriorated crystals, while the texture of the top layer ice has always been reported as granular (Carnat et al., 2013; Perovich et al., 2009).

3.2. Sea Ice Salinity

Sea ice traps salt as it grows, and the desalination processes in the subsequent growth and melt seasons cause the sea ice salinity to decrease over time. FYI has a "C-shaped" vertical salinity profile in the growth season but shows a low salinity at the surface in the melt season due to the meltwater flushing (Notz & Worster, 2009). Our FYI samples showed a low-salinity (<1.0 psu) top layer and approximately 3.0 psu salinity at the bottom. The low-salinity ice made up 0–50% of the ice cores with an average of 25 ± 12%. Carnat et al. (2013) and Tucker et al. (1987) reported similar shapes of FYI salinity profiles but with slightly higher level. MYI is less saline and characterized by a fresh top layer because extensive desalination has already occurred during previous seasons (Vancoppenolle et al., 2006). Our MYI samples exhibited a nearly fresh (<0.5 psu) upper layer and approximately 2.0 psu salinity in the bottom layer, resembling the model of Vancoppenolle et al. (2006) and the observations of Eicken et al. (1995) and Tucker et al. (1987). Furthermore, the nearly fresh layer accounted for 14–56% of the sampled MYI thickness with an average of 30 ± 9%.

Currently, in several widely used sea ice models, for example, Bitz and Lipscomb (1999) and Hunke and Lipscomb (2008), the vertical profile of salinity is a prescribed function of normalized ice depth. To better depict our salinity profiles and compare with this prescribed function, the normalized ice depth was also employed here. The thickness of an ice core was divided into 10 even layers, and the sea ice salinity of each layer was averaged by weighting with the section length (Figure 4). The salinity increased overall along the depth for both ice types. At the top of MYI it was 0.1 ± 0.2 psu, slightly lower than in FYI (0.5 ± 0.6 psu). The salinity parameterization used in Bitz and Lipscomb (1999) and Hunke and Lipscomb (2008) was based on the MYI salinity profile derived from Schwarzacher (1959), shown as the blue dashed line in Figure 4. Schwarzacher's measurements were conducted from 40 Arctic ice cores taken from May to September 1958. The salinity ranged between 0.1 and 4.0 psu from ice surface to the depth of 300 cm. The general formula of Schwarzacher's salinity profile is

$$S(z) = \frac{1}{2} S_{\max} \left[1 - \cos\left(\pi z^{\left(\frac{a}{z+b}\right)}\right)\right] \tag{1}$$

where S is the salinity, z is the normalized depth within the interval [0, 1], and a, b are the fit parameters. Assuming $a, b \neq 0$, this formula gives $S(0) = 0$, $S(1) = S_{\max}$. The best fit in Bitz and Lipscomb (1999) and Hunke and Lipscomb (2008) was $S_{\max} = 3.2$ psu, $a = 0.407$, $b = 0.573$. Our data showed much lower salinities, and the best fit parameter values were $S_{\max} = 2.2$ psu, $a = 2.32$, $b = 2.67$, with a slightly modified curvature (red dashed line in Figure 4b). The coefficient of determination (R^2) was 0.99, and the significance level (p) was less than 0.01. The salinity profile with adjusted $S_{\max} = 2.2$ psu and unadjusted a and b was also compared with our observation (not shown), which showed a large deviation from our observations, especially in the middle part of the cores. Another formula for the MYI salinity profile reported in Eicken et al. (1995) using a cubic polynomial is also presented in Figure 4b. This profile was derived from 66 cores sampled at undeformed MYI with mean thickness of 2.86 m in the ASA in August and September 1991. Compared with our measurements, the salinity profile reported in Eicken et al. (1995) also has higher level.

The Arctic is undergoing a transition from a predominantly MYI system to a FYI system (Maslanik et al., 2007). However, to the authors' best knowledge, only a few parameterizations have been developed for FYI salinity profiles during the melt season. It is valuable to show and parameterize the vertical profile of FYI salinity for sea ice models. In this paper, we have established a FYI salinity formulation similar to that of MYI, but with modifications to give a positive limit at $z = 0$. The new formula is

$$S(z) = \frac{1}{2} S_{\max} \left[1 - \cos\left(\pi z^{\left(\frac{a}{z+b}\right)}\right)\right] + S(0) \tag{2}$$

The best fit to the observations was obtained with $S_{\max} = 2.5$ psu, $a = 0.76$, $b = 0.58$, $S(0) = 0.41$ psu, and the goodness of fit was $R^2 = 1.00$, $p < 0.01$. The fitted profile is plotted as the red dashed line in Figure 4a. It is noteworthy that the salinity has a stronger temporal variability in FYI than in MYI and that the FYI salinity profile is quite different in the melt season from that in the growing season. Therefore, the formula in Equation 2 is appropriate only for summer FYI.

The bulk salinity of the individual ice cores ranged between 0.4 and 3.2 psu with an average of 1.9 ± 0.6 psu for FYI and from 0.4 to 2.4 psu with a mean of 1.3 ± 0.5 psu for MYI. Furthermore, the distributions of the bulk salinity for both FYI and MYI conformed to normal distribution inspected using the Shapiro-Wilk test ($p = 0.05$) (Razali & Wah, 2011). A linear dependence of the bulk salinity on ice thickness in summer has been reported in previous works (Eicken et al., 1995; Overgaard et al., 1983; Tucker et al., 1987). In this study, a stronger positive correlation was found for FYI with $R^2 = 0.48$ (Figure 5a), whereas a weaker relationship was obtained for MYI with $R^2 = 0.37$ (Figure 5b). The previous correlations from Eicken et al. (1995), Overgaard et al. (1983), and Tucker et al. (1987) are also presented in Figure 5 (colored lines), which show higher levels than our observations. It is noteworthy that the correlation between the bulk salinity and ice thickness for FYI was much higher in our data than in Overgaard et al. (1983) ($R^2 = 0.01$). A possible explanation is that our warmer ice with enhanced permeability leaks brine more than in the previous studies from the

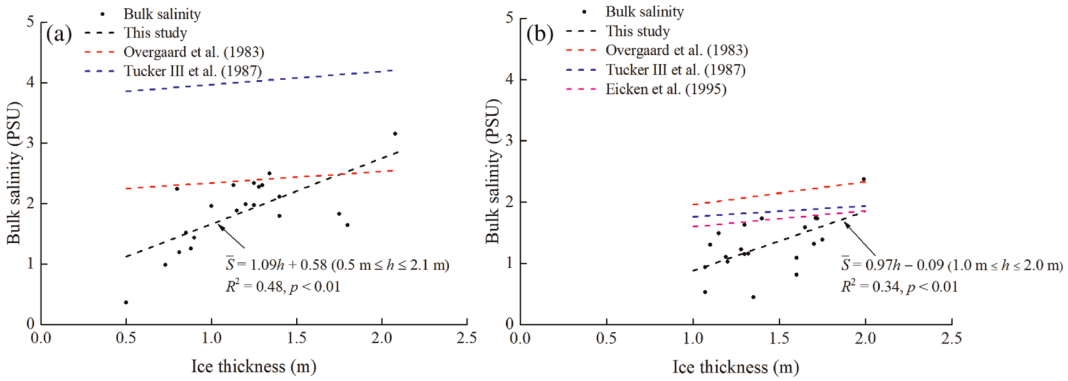

Figure 5. Sea ice bulk salinity ($\bar{S}$) versus ice thickness (h) (solid points) and regression lines (black dashed lines) with equations, coefficients of determination (R^2), and significance level (p) for (a) FYI and (b) MYI. Also shown are the regression lines reported in previous studies (colored dashed lines).

late 1900s. This is true especially for thin ice, whereas thick ice has still cold core, and the brine drainage is less than in thin ice. Additionally, different durations and locations of ice sampling may also be attributed to the different correlation coefficient.

3.3. Sea Ice Temperature

The ice temperature of the samples ranged between −3.1 and −0.1 °C for FYI and between −2.5 and −0.1 °C for MYI. To better depict the general variations of ice temperature profiles in late summer and to keep consistency with the analysis of ice salinity, a core was also divided into 10 even layers, and the mean temperature of each layer was determined assuming a linear variation of temperature between two measurement points and weighted by the distance of the points. Ice cores sampled in 2018 were excluded here because of delayed measurements after sampling leading to unrealistically high values at some upper measurement points. Sea ice temperature is usually affected by snow on ice, air temperature, solar radiation, and ice

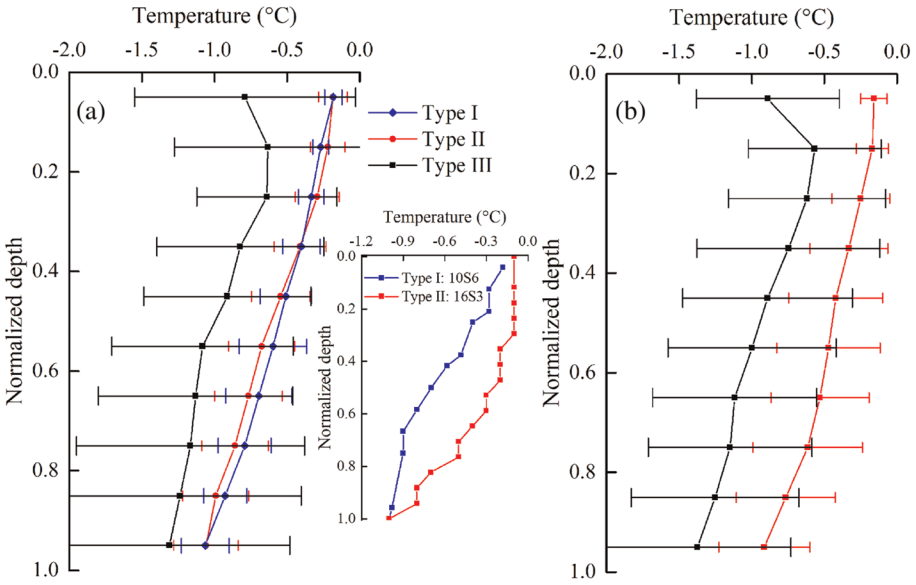

Figure 6. Mean sea ice temperature against normalized depth for (a) FYI and (b) MYI during the melt season. The error bars represent the standard deviations, and the subplot in (a) is the typical examples of Type I and II profiles of individual cores.

growth/melt histories. Considering the thin snow layers and their porous structure in the sampled ice sites, the snow insulation effect on sea ice temperature is expected to have been weakened. In general, sea ice warms to the freezing point in summer; however, three types of ice temperature profiles were further identified in Figure 6.

As reported in many previous studies (Carnat et al., 2013; Tucker et al., 1987), there is a more common type of ice temperature profile with a linear decrease from surface to bottom (Type I). The vertical temperature gradient was estimated using the temperature difference between the ice surface and the bottom divided by the ice thickness, giving the mean gradient of −1.0 °C/m. However, more of our cases, half of the FYI and 42% of the MYI samples, had an isothermal layer close to 0 °C in the upper ice sheet (Type II), corresponding to the low-salinity layer in the top part. There is a large overlap between the mean ice temperature profiles of Type I and II because the difference was hidden to some degree by the averaging. To make the difference clear, a subplot with typical examples of Type I and II profiles of individual cores is inserted in Figure 6a, showing well the isothermal layer near 0 °C in the top part of Type II profile. Furthermore, the air temperature corresponding to Type II profiles was slightly higher than in the case of Type I profiles. Type III profile also had an evident positive-gradient layer in the surface ice section. A similar ice temperature profile was observed by Overgaard et al. (1983). This is because the absorbed solar radiation in ice heats the subsurface, while the surface temperature of ice decreases due to the longwave radiation losses (Cheng et al., 2003). The bulk temperature of both ice types was also determined. For FYI, the bulk temperature ranged between −2.7 and −0.3 °C with an average of −0.8 ± 0.6 °C. Since MYI is less saline, it had a narrow bulk temperature range from −1.7 to −0.2 °C with a mean of −0.7 ± 0.4 °C.

3.4. Sea Ice Density

The sea ice density was lower in the upper part of the ice sheet than in the bottom part corresponding closely to the concentration of air-filled pores, which originated from the surface layer melting process. The density of the freeboard (the ice section above the sea level) of the ice cores ranged from 491 to 874 kg/m^3 for FYI and 521 to 885 kg/m^3 for MYI, with averages of 718 ± 87 kg/m^3 and 701 ± 86 kg/m^3, respectively. The density of the draft (the ice section below the sea level) ranged between 583–907 kg/m^3 for FYI and 690–906 kg/m^3 for MYI, with averages of 804 ± 80 kg/m^3 and 825 ± 52 kg/m^3, respectively. The FYI bulk density ranged between 600 and 900 kg/m^3 with an average of 793 ± 74 kg/m^3, and the bulk density of MYI measured 686–903 kg/m^3 with an average of 810 ± 49 kg/m^3. The measurements of sea ice density using the same technique in other studies are compared in Table 2. Our upper limit of density was similar to the earlier reported values, but our samples showed a smaller lower limit. That is, we obtained a wider range of ice density than before. Both different measurement uncertainties and growth/melt histories of ice samples can partly contribute to the variability.

Sea ice density increased with depth due to the reduced gas content. Eicken et al. (1995) reported a similar shape of the mean density profile for summer MYI from 14 ice cores and adopted a logarithmic formula for fitting:

$$\rho(z_i) = 35.7 \times \ln(z_i) + 881.8 \tag{3}$$

where ρ is the ice density (kg/m^3), and z_i is the real ice depth (m). This equation does not work in the limit as $z_i \to 0$. Therefore, a quadratic polynomial was used here:

$$\rho(z) = Az^2 + Bz + \rho(0) \tag{4}$$

where $\rho(0)$ is the density of ice at the surface and the parameters A and B are constants. To keep consistency with the salinity parameterization, the normalized depth was also used in Equation 4; the ice thicknesses of our sampled cores were divided into 10 even layers, and the density of each layer was averaged using the measurement section length as the weight. We obtained the following parameter values:

1. FYI: $A = -103.4$ kg/m^3, $B = 231.5$ kg/m^3, $\rho(0) = 710.1$ kg/m^3 ($R^2 = 0.99$ and $p < 0.01$).
2. MYI: $A = -218.1$ kg/m^3, $B = 423.1$ kg/m^3, $\rho(0) = 672.5$ kg/m^3 ($R^2 = 0.98$ and $p < 0.01$).

The fit by Eicken et al. (1995) is presented in Figure 7b (blue dashed line) for a comparison. It is clear that it does not match our observations, especially in the upper part of the ice sheet.

Table 2
Comparison of the Observed Sea Ice Density With Earlier Reported Values Using the Same Technique

	Bulk density (kg/m^3)		
Reference	Entire length	Above sea level	Below sea level
Forsström et al. (2011)	901.9		
Timco and Frederking (1996)	700–940	840–910 for FYI 720–910 for MYI	900–940
Eicken et al. (1995)	857–922		
Perovich et al. (2009)		700–800	850–910
This study	600–900 for FYI 686–903 for MYI	491–874 for FYI 521–885 for MYI	583–907 for FYI 690–906 for MYI

Note. Density in Eicken et al. (1995) was derived from MYI samples and in others was derived from both FYI and MYI samples.

4. Discussion

4.1. Sea Ice Brine and Gas Volume Fractions

Gas bubbles and brine pockets are two primary optically active impurities of sea ice (Light et al., 2004). Brine and gas inclusions are trapped within the ice when ice forms. The brine salinity and volume are determined by the phase equilibrium, which depends on the temperature (Cox & Weeks, 1983). At the same time, gas bubbles are expected to form in brine inclusions (Crabeck et al., 2016; Light et al., 2003). In addition, the drained brine pockets in the freeboard are replaced by air in summer. The changes in gas and brine contents, in turn, affect the optical properties of sea ice. The distributions of brine and gas inclusions are not precisely known, since they are difficult to measure directly in the field. Mathematical formulae exist to evaluate their volume fractions when the temperature, salinity, and density are known, as shown for below −2 °C by Cox and Weeks (1983) and for the interval (−2, 0) °C by Leppäranta and Manninen (1988). The ice cores were divided into 10 layers, as described in section 3, and the average ice temperature, salinity, and density in each layer were determined. These values were then used to estimate the brine and gas volume fractions (v_a and v_b) in each ice layer, and the distribution characteristics of brine and gas within summer Arctic sea ice could then be explored in a quantitative way.

The uncertainties of the measured density and salinity are two main error sources of the estimated v_a and v_b. The error caused by density uncertainty can be evaluated quantitatively using error propagation. The maximum uncertainty of density is taken as the sum of measurement uncertainty (±5%) and the upper limit of the uncertainty due to brine drainage (−20%). Taking the mean bulk temperature, salinity, and density of all ice cores of −0.8 °C, 1.6 psu, and 801.4 kg/m^3, respectively, gives a maximum underestimation of v_b by 15–25% and a maximum overestimation of v_a by 96–160%. The measured salinity is also underestimated because of the brine loss, which further underestimates v_a and v_b. Given that FYI samples were just slightly more saline than MYI and the salinity uncertainty of MYI is only a few tenths on average (Eicken et al., 1995), the underestimation caused to v_b was small and even less to v_a for both FYI and MYI.

The estimated brine content of our samples ranged between 0% and 61.8% for FYI and between 0% and 37.3% for MYI. The FYI bulk v_b ranged between 3.0% and 25.9% with an average of 11.3 ± 6.2%, while for MYI the corresponding range and average were 2.2–21.4% and 9.5 ± 11.0%, respectively. To better depict the vertical variation of v_b, the mean value of each layer was plotted against the normalized depth. Typically, both FYI and MYI had v_b profiles with a reversed "C-shape" with a maximum in the middle. Similar vertical profiles have been reported in Carnat et al. (2013) and Overgaard et al. (1983) for melting fast ice and MYI, respectively, while a profile showing decreasing v_b with depth was reported in Eicken et al. (1995) because of a relatively low ice temperature. The simple mathematical equations using quadratic polynomials could parameterize the general variations of v_b for both ice types, which were shown in Figure 8 with high R^2.

The gas content in our samples ranged between 0% and 65.4% for FYI and between 0% and 34.4% for MYI. The FYI bulk value range was 2.7–35.4% with a mean value of 14.9 ± 7.9%, and for MYI the corresponding range and average were 3.6–26.1% and 13.5 ± 12.7%, respectively. The mean v_a was plotted against the

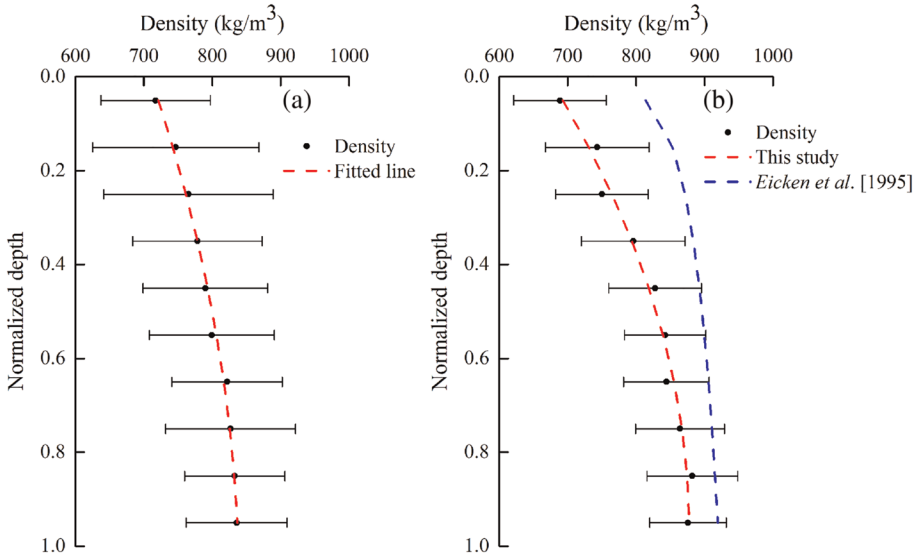

Figure 7. Mean sea ice density versus normalized depth (solid points) for (a) FYI and (b) MYI during the melt season. The error bars represent the standard deviations. The red dashed lines are the current fitted lines, and the MYI profile by Eicken et al. (1995) is shown by the blue dashed line.

normalized depth (Figure 9). It was highest (>20%) in the top layer of both FYI and MYI, reflecting the intense interaction between atmosphere and ice surface. The v_a decreased to approximately 10% at the bottom of both FYI and MYI. A similar vertical profile was also reported by Eicken et al. (1995) for summer MYI showing that v_a decreased from >20% at the top to <5% at the bottom, although there was also an overestimation of v_a compared with the in situ value due to the underestimated density caused by brine drainage during core drilling and measurement uncertainty. A quadratic polynomial was used here to fit the varying trend of v_a (Figure 9).

Permeability is the key factor affecting the hydrological evolution of summer sea ice (Eicken et al., 2002). The percolation threshold v_b^* depends on the crystal structure; at $v_b > v_b^*$, brine or sea water can move through the ice (Golden et al., 1998, 2007). For columnar sea ice, $v_b^* = 5\%$; however, no specific value is available for the other crystal types. Columnar ice accounted for the largest portion in the ice cores, and we therefore assumed the percolation threshold as 5% (red lines in Figure 8) for the whole ice sheet. As shown in Figure 8, layers with $v_b < 5\%$ existed at the top of both FYI and MYI, accounting for approximately 10% and 22% of the ice thickness, respectively. The lower sections were permeable with $v_b > 5\%$. It is noteworthy that (Figure 9) v_a in the top low-brine layers was higher than 5% (v_a still can be >5% if the overestimation is removed) because the brine had already drained out. These sections had been permeable through the brine channels and were probably still permeable via the gas pores (or air-filled brine channels). In other words, both FYI and MYI were completely permeable through the whole depth.

The gas inclusions of summer sea ice can form in the well-drained brine pockets above the waterline and in the brine inclusions as the ice walls surrounding brine pockets melt (Light et al., 2003). Therefore, the ratio of gas and brine contents may differ along the ice depth. Their profiles from an individual ice core were compared (see representative examples in Figure 10): in most cases, 57% for FYI and 62% for MYI, the brine volume fraction was less than the gas volume fraction in the upper part of the ice sheet, while the opposite was true deeper. The turning points were located at the normalized depth range of 0.22–0.67 for FYI and 0.22–0.78 for MYI. For the rest of the sites, the gas volume fraction was greater than the brine volume fraction across the whole ice sheet. The relationship between the bulk gas and brine volume fractions was also examined, showing a weak negative correlation with correlation coefficients of −0.13 and −0.11 for FYI and MYI, respectively.

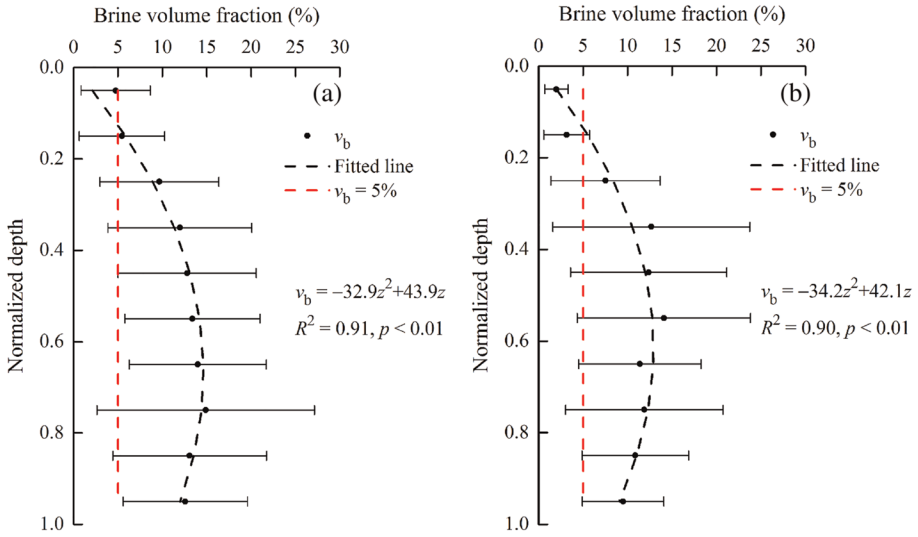

Figure 8. Mean brine volume fraction versus normalized depth (solid points) for (a) FYI and (b) MYI and the corresponding fitted lines (black dashed lines). The error bars represent the standard deviations. Also shown are red lines representing $v_b = 5\%$, the equations of the fitted lines, goodness of fit (R^2), and significance level (p).

4.2. Estimation of the Energy for Melting Sea Ice

The energy for melting sea ice is the energy required to melt a unit volume of sea ice completely (Bitz & Lipscomb, 1999). It depends on the brine and gas inclusions. As the ice warms, the brine salinity must decrease by melting the walls surrounding the brine pockets. The energy for complete melting of sea ice includes the heat to raise the temperature of pure ice, to raise brine temperature, and to melt ice crystals. In addition, for summer sea ice, gas can occupy a significant fraction, which further decreases the energy of melting. A semiempirical formula to calculate the latent heat of fusion for sea ice was given by Yen (1981), but it can become problematic for warm sea ice because of the strong nonlinearity in the phase composition when the ice temperature approaches 0 °C (Leppäranta & Manninen, 1988). An alternative approach to Yen (1981) is to start from the definitions and take care that the formulae behave properly as $T \to 0$ °C, $S \to 0$ psu. The energy of complete sea ice melting is

$$L = (\rho_i L_i - \rho_i c_i T)[1-(v_a + v_b)] - \rho_b c_b v_b T \tag{5}$$

where the lower indexes i and b refer to pure ice and brine, respectively; L is the energy for complete sea ice melting; $L_i = 335$ kJ/kg is the latent heat of fusion of pure ice; $c_i = 2.1$ kJ/(kg · °C) is the specific heat of pure ice; $c_b \approx 4.0$ kJ/(kg · °C) is the specific heat of brine (assumed equal to the seawater value here); T is the ice temperature (°C); and ρ_i and ρ_b are the densities of pure ice and brine, respectively. The densities are given in kilograms per cubic meter by

$$\rho_i = 917 - 0.1403 \times T \tag{6}$$

$$\rho_b = 1000 + 0.82 \times S_b \tag{7}$$

The brine volume depends on the brine salinity $S_b = S_b(T)$, and it has the limit $S_b \to 0$ psu as $T \to 0$ °C. To reach this limit properly, we have taken the formulation of Assur (1960) for the brine salinity of warm summer sea ice ($T > -8$ °C):

$$S_b = \frac{T}{T - 54.11} \times 1000 \tag{8}$$

where S_b is the salinity of brine in practical salinity unit.

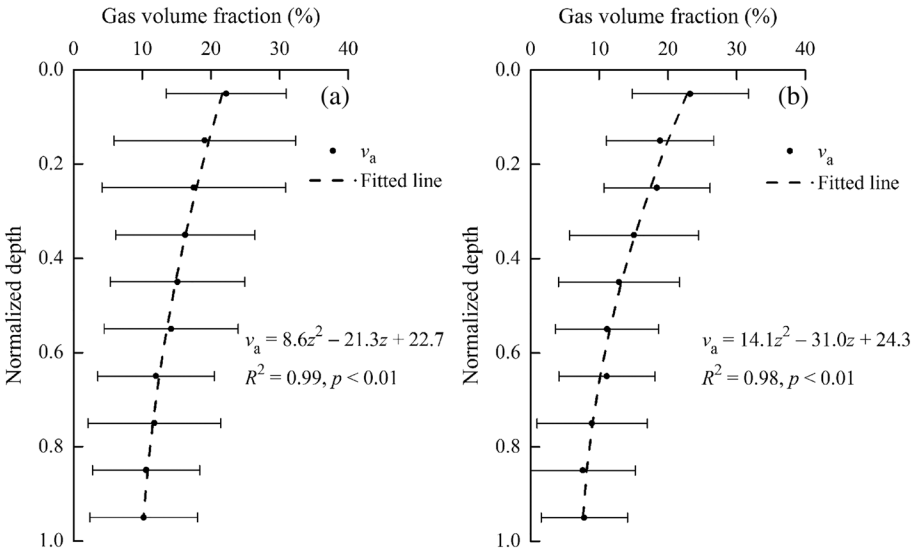

Figure 9. Mean gas volume fraction versus normalized depth (solid points) for (a) FYI and (b) MYI and the corresponding fitted lines (dashed lines). The error bars represent the standard deviations. Also shown are the equations of the fitted lines, goodness of fit (R^2), and significance level (p).

With the measured triple (T, S, ρ), the energy for complete melting in the individual sea ice layers was estimated and then integrated as the representative energy for the complete melting of the entire ice core. For FYI, the energy for melting was (1.71–2.78) × 10^5 kJ with an average of (2.26 ± 0.29) × 10^5 kJ. Similar range and average were obtained for MYI: (1.83–2.69) × 10^5 kJ and (2.36 ± 0.24) × 10^5 kJ, respectively. Given the comparisons with the previously reported Arctic sea ice properties above, the energy for sea ice melting is likely to have changed for the present Arctic, especially for MYI. If we assume ice density as the widely used value of 910 kg/m^3 and salinity as the average derived from Schwarzacher's profile (2.3 psu), the energy for melting equals 2.50 × 10^5 kJ under the same mean temperature for our MYI samples. Therefore,

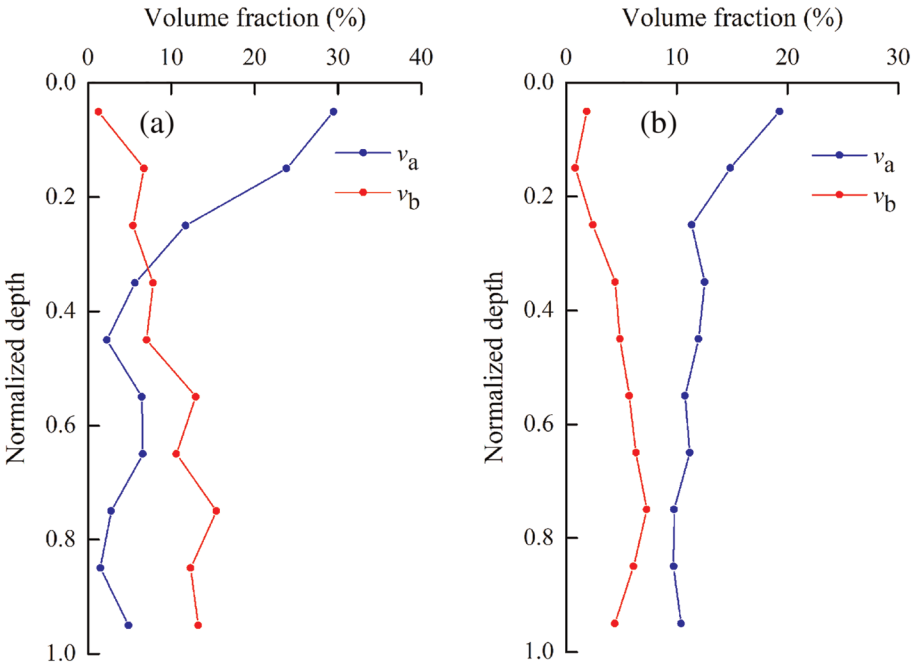

Figure 10. Comparison between the profiles of v_a and v_b from individual ice cores: (a) 12-S6 and (b) 08-S4.

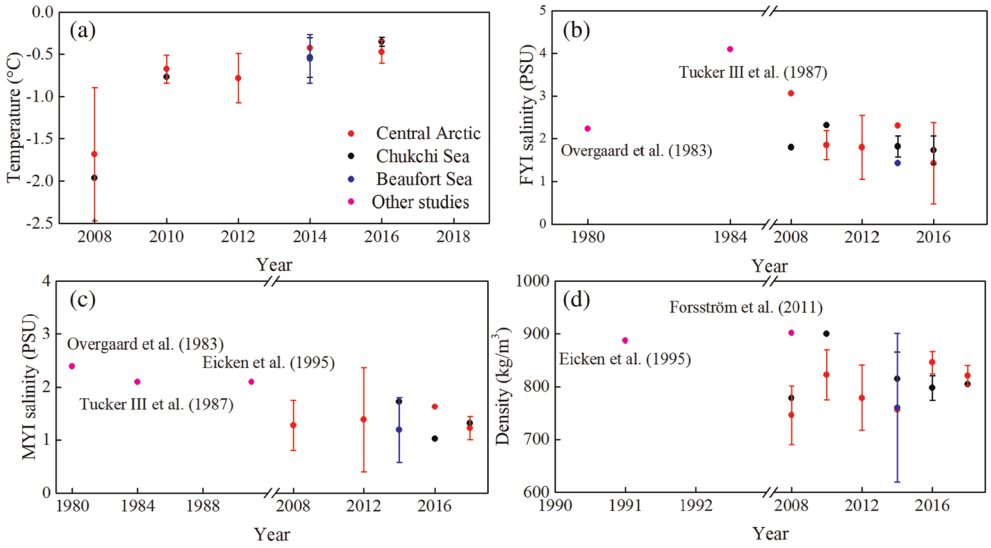

Figure 11. Interannual variability in the annual summer average of the (a) bulk ice temperature, salinity of (b) FYI and (c) MYI, and (d) density. The error bars represent the standard deviations. The data points in this study without error bars indicate those with only one measurement site located in the study area. Also shown are the mean salinity and density from other field observations. The density in Forsström et al. (2011) was derived from samples collected during 2000–2008.

approximately 6% less energy is required to melt a unit volume of MYI under the current Arctic status than before. The difference may be less because of the overestimation of porosity for our samples. In combination with the reduction in Arctic sea ice thickness and surface albedo, the decreased energy for sea ice melting can further increase the amount of solar energy absorbed by the upper ocean during summer. However, this effect is probably small compared with the other processes to increase the energy absorbed by the upper ocean. The additional heat stored in the upper ocean can warm sea ice and lower the ice growth rate in the early growing season and delay the autumn freeze up. An increased sea surface temperature can enhance the evaporation rate that would further warm the lower atmosphere and increase the boundary layer cloud production (Boisvert & Stroeve, 2015).

4.3. Interannual Comparison of Sea Ice Physical Properties

Due to the sparse field data, only a few reports are available on the interannual variability of the physical properties of sea ice. The CHINARE data from the Chukchi Sea, Beaufort Sea, and Central Arctic provide an opportunity to gain an insight into the interannual variations of the Arctic summer sea ice. The results are shown in Figure 11.

The annual averages of the sea ice properties were derived from the cores sampled on different dates and at different locations that makes the dataset scattered. However, some general trends are still clear. The summer ice temperature in the Chukchi Sea and Central Arctic increased year by year. Ice temperature was relatively low in 2008 because the sampling was near the end of the melt season and air temperature began to drop. Ice temperature increased to above −1.0 °C after 2010. FYI showed a slight decrease in salinity from 2008 to 2018. Many factors can affect this trend, such as the surface water salinity at the time of ice formation, the brine drainage process related to ice temperature gradient during winter, and the flushing caused by the surface melt as well as snow melt during summer. But it is difficult to determine which processes dominate the trend. Conversely, MYI salinity did not show a similar temporal tendency because extensive desalination had already occurred during previous seasons, resulting in minor further changes. The ice density in the Chukchi Sea and Central Arctic also showed less variability between 2008 and 2018.

Furthermore, the previously reported salinity and density are also plotted in Figure 11. Salinity was typically higher in the previous studies. In addition to the potentially different ice growth and melt histories, the

variability of ice salinity may also be partly attributed to the decreased ice thickness in our observations. Ice thickness in Eicken et al. (1995) was 2.86 ± 0.99 m, in Tucker et al. (1987) it was 0.38–2.36 m for FYI and 1.74–5.36 m for MYI, and in Overgaard et al. (1983) it was approximately 1–3 m for FYI and 2–5 m for MYI, all of which are much higher than the thickness of ice in our samples. Brine can drain out of the thinner ice more easily leading to a decreased salinity. Besides, these literature salinities were derived from ice samples in the ASA. The relatively high sea surface salinity in the ASA compared with PSA during ice freeze-up season could also contribute to the high literature values (Garcia-Eidell et al., 2017). Density values reported in Eicken et al. (1995) and Forsström et al. (2011) were also greater than our observations. Their samples collected in the ASA could trap much salt and thus increase the ice density. The different measurement uncertainties can also cause the variability.

5. Conclusions

Comprehensive sea ice surveys were carried out in the Chukchi Sea, Beaufort Sea, and Central Arctic during the melt seasons of 2008–2018 through the CHINARE programs. A total of 41 ice stations was visited. Twenty one of the surveys were carried out on FYI and 20 on MYI floes. Ice cores were sampled at each station for the ice temperature, salinity, density, and crystal structure analyses.

During the melt seasons over the years 2008–2018, the bulk salinity of FYI was 1.9 ± 0.6 psu, which is 0.5 psu less than in Overgaard et al. (1983) and 2.1 psu less than in Tucker et al. (1987); the bulk salinity of MYI was 1.3 ± 0.5 psu in this study, approximately 1.0 psu lower than the values reported by the previous studies (Overgaard et al., 1983; Tucker et al., 1987). The bulk density was 793 ± 74 kg/m^3 for FYI and 810 ± 49 kg/m^3 for MYI, lower than the previously reported average of 910 kg/m^3 in Timco and Frederking (1996). The previously applied parameterizations for MYI salinity (Hunke & Lipscomb, 2008) and density (Eicken et al., 1995) show higher levels than our observations and thus have been here updated based on the new field data (Figures 4 and 7).

The Arctic Ocean is undergoing a transition from a predominantly MYI system to a FYI system. Therefore, the vertical profiles of salinity and density for FYI in late summer presented here illustrate the changing in the properties of sea ice, and their simple existing parameterization were taken here for revision to be employed in future research modeling. Sea ice becomes porous as it warms. The bulk brine volume fraction v_b ranged within 3.0–25.9% for FYI and 2.2–21.4% for MYI, and the bulk gas volume fraction v_a ranged between 2.7–35.4% for FYI and 3.6–26.1% for MYI. The variability in both v_b and v_a along the vertical was described by polynomials (Figures 8 and 9). Gas occupied more volume in the decaying sea ice than brine, especially in the upper part of ice. In general, the porosity of late summer sea ice reached 20–30% through most of the length of the ice cores.

The effects of the atmosphere-ice interaction on the summer ice is suggested from the surface characteristics of the vertical profiles of the sea ice properties. A possible scenario is that surface ablation deteriorates the top layer ice with retexturing (approximate 10% of both FYI and MYI thickness); the pressure overhead of the meltwater drove the brine down that partly caused the low-salinity surface layer in the ice (25% of FYI thickness and 30% of MYI thickness); the drained brine pockets in the top layer were refilled by air, further decreasing the surface ice density (especially in the freeboard).

Arctic sea ice undergoes continuous changes. The present study has revealed very different sea ice physical properties compared with observations dating back over decades, especially for MYI. This provides a valuable insight for sea ice numerical simulations, and the results can be used for model calibration and initialization. First, the parameterizations of sea ice physical properties used in models (e.g., salinity and density) derived from the previous studies are biased with respect to the present Arctic sea ice. Therefore, an update is required. Second, because a large fraction of summer sea ice is occupied by gas and brine, their variability in sea ice should be fully considered. The mushy-layer theory has been applied to brine dynamics within sea ice and has proved to be successful (Feltham et al., 2006). However, a similar consideration of gas bubbles in sea ice has been absent so far because of the many unknown physical mechanisms of gas bubble dynamics. Finally, Arctic is transitioning from a predominantly MYI system to a FYI system, and thus, the revision of parameterizations of sea ice physical properties is necessary for both FYI and MYI and serves as the basis for future research.

Appendix A: Details of Ice Stations

A total of 41 ice stations were selected in the expeditions during the summers of 2008–2018. The detailed information of the ice stations is summarized in Table A1.

Table A1
The Specific Information of Ice Stations

ID	Date	Location	Ice thickness (cm)	Snow thickness (cm)	Freeboard (cm)	Bulk properties			Air temperature (°C)	Ice age
						Ice temperature (°C)	Salinity (psu)	Density (kg/m^3)		
08-S1	2008-8-27	85.1°N, 147.1°W	160.7 ± 9.0	N/R	N/R	−0.8 ± 0.4	1.1 ± 0.8	723 ± 29	−0.5	MYI
08-S2	2008-8-28	85.2°N, 147.3°W	160.0 ± 0	N/R	N/R	−1.7 ± 0.2	0.9 ± 0.7	769 ± 48	−2.8	MYI
08-S3	2008-8-31	83.0°N, 150.9°W	205.3 ± 4.6	N/R	N/R	−2.7 ± 0.2	3.2 ± 0.7	682 ± 38	−4.2	FYI
08-S4	2008-9-1	81.0°N, 155.3°W	168.0 ± 6.9	N/R	N/R	−1.6 ± 0.6	1.8 ± 1.1	810 ± 33	−2.6	MYI
08-S5	2008-9-2	79.9°N, 162.8°W	76.7 ± 5.8	N/R	N/R	−2.0 ± 0.5	2.2 ± 1.3	779 ± 109	−4.0	FYI
10-S1	2010-7-30	77.5°N, 158.9°W	140.0 ± 0	5.5	20	−0.8 ± 0.4	2.1 ± 1.3	900 ± 27	−0.5	FYI
10-S2	2010-8-1	80.5°N, 161.3°W	135.7 ± 5.1	12	15	−0.8 ± 0.3	1.8 ± 1.1	855 ± 42	0.5	FYI
10-S3	2010-8-3	82.5°N, 165.6°W	173.3 ± 2.9	12	16	−0.8 ± 0.5	1.8 ± 0.9	838 ± 68	−0.2	FYI
10-S4	2010-8-4	84.2°N, 167.1°W	121.7 ± 2.9	11	10	−0.8 ± 0.4	2.0 ± 1.0	863 ± 61	−1.6	FYI
10-S5	2010-8-19	88.4°N, 177.2°W	121.7 ± 5.8	10	11	−0.7 ± 0.4	1.9 ± 1.2	823 ± 50	−0.2	FYI
10-S6	2010-8-22	83.7°N, 170.7°W	120.7 ± 4.0	8.5	10.5	−0.6 ± 0.3	2.3 ± 1.4	826 ± 38	−1.5	FYI
10-S7	2010-8-23	82.0°N, 169.0°W	86.0 ± 1.7	7.0	7.5	−0.4 ± 0.4	1.3 ± 0.6	731 ± 54	0.4	FYI
12-S1	2012-8-29	86.5°N, 120.3°E	107.7 ± 4.6	11	7	−1.2 ± 0.4	2.3 ± 0.8	786 ± 41	−2.9	FYI
12-S2	2012-8-30	87.4°N, 123.0°E	128.3 ± 5.8	15	12	−0.4 ± 0.3	0.4 ± 0.5	793 ± 97	−0.2	MYI
12-S3	2012-8-31	86.4°N, 120.2°E	73.3 ± 3.5	17	3	−0.6 ± 0.2	1.0 ± 0.7	665 ± 62	−1.2	FYI
12-S4	2012-9-1	84.6°N, 145.2°E	183.3 ± 14.3	20	12	−0.9 ± 0.4	2.4 ± 1.1	827 ± 60	−1.6	MYI
12-S5	2012-9-1	84.1°N, 158.5°E	126.0 ± 1.7	13	8	−0.9 ± 0.4	2.3 ± 1.3	773 ± 88	−2.1	FYI
12-S6	2012-9-2	83.4°N, 161.4°E	172.3 ± 2.5	9	12	−0.7 ± 0.3	1.4 ± 1.0	839 ± 74	−3.1	MYI
14-S1	2014-8-10	76.7°N, 151.1°W	169.0 ± 2.6	7	17	−0.9 ± 0.4	1.7 ± 0.8	903 ± 57	−2.2	MYI
14-S2	2014-8-11	77.2°N, 154.6°W	104.7 ± 4.0	5	14	−0.2 ± 0.2	0.5 ± 0.3	849 ± 109	1.4	MYI
14-S3	2014-8-13	77.5°N, 163.1°W	183.3 ± 15.3	11	12	−0.8 ± 0.3	1.6 ± 0.6	812 ± 41	−1.2	FYI
14-S4	2014-8-14	78.3°N, 161.0°W	120.0 ± 0	7	12	−0.5 ± 0.3	2.0 ± 1.3	868 ± 78	2.6	FYI
14-S5	2014-8-16	79.9°N, 158.6°W	140.0 ± 0	7	12	−0.3 ± 0.3	1.7 ± 1.1	764 ± 91	3.6	MYI
14-S6	2014-8-17	80.9°N, 157.6°W	120.0 ± 17.3	8	10	−0.4 ± 0.3	2.3 ± 1.6	756 ± 55	3.1	FYI
14-S7	2014-8-28	80.0°N, 152.6°W	98.7 ± 8.1	2.7	6	−0.5 ± 0.3	1.4 ± 1.3	600 ± 146	−0.4	FYI
14-S8	2014-8-28	78.8°N, 149.4°W	106.7 ± 5.8	14	13	−0.5 ± 0.3	1.3 ± 1.1	686 ± 46	0.8	MYI
16-S1	2016-8-4	79.0°N, 169.2°W	82.2 ± 2.6	7.5	N/R	−0.4 ± 0.1	1.5 ± 1.1	804 ± 81	0.8	FYI
16-S2	2016-8-5	80.1°N, 169.0°W	136.0 ± 2.6	6	10.7	−0.5 ± 0.2	2.5 ± 1.1	856 ± 44	−1.1	FYI
16-S3	2016-8-6	81.5°N, 167.7°W	82.8 ± 2.0	5	4	−0.4 ± 0.3	1.2 ± 0.9	815 ± 137	1.1	FYI
16-S4	2016-8-7	82.3°N, 168.1°W	49.3 ± 1.2	4.6	3.8	−0.4 ± 0.3	0.4 ± 0.8	847 ± 71	−0.8	FYI
16-S5	2016-8-8	82.6°N, 167.0°W	126.7 ± 5.8	6	14	−0.6 ± 0.3	1.6 ± 1.1	865 ± 114	−2.6	MYI
16-S6	2016-8-17	79.9°N, 179.3°W	114.3 ± 12.5	2.5	14	−0.3 ± 0.2	1.0 ± 0.7	818 ± 86	−1.0	MYI
16-S7	2016-8-20	76.3°N, 179.6°W	107.0 ± 19.9	5	7.5	−0.3 ± 0.2	2.0 ± 1.1	772 ± 67	−0.9	FYI
18-S1	2018-8-12	79.9°N, 169.1°W	147.5 ± 31.8	9.3	8	N/R	1.3 ± 1.4	805 ± 108	−1.4	MYI
18-S2	2018-8-13	81.2°N, 169.4°W	111.5 ± 4.9	16.3	5.8	N/R	1.4 ± 1.4	840 ± 78	−0.4	MYI
18-S3	2018-8-14	82.0°N, 168.2°W	152.5 ± 17.7	7.5	13.8	N/R	1.6 ± 1.2	831 ± 93	0.2	MYI
18-S4	2018-8-14	83.6°N, 167.4°W	128.0 ± 0	6	3.4	N/R	1.2 ± 1.1	844 ± 89	1.0	MYI
18-S5	2018-8-20	84.7°N, 166.0°W	106.0 ± 1.4	2.6	6.6	N/R	0.9 ± 0.8	789 ± 110	0.0	MYI
18-S6	2018-8-21	84.7°N, 167.7°W	141.0 ± 12.7	8	4.6	N/R	1.2 ± 1.4	820 ± 77	0.1	MYI
18-S7	2018-8-23	84.6°N, 162.2°W	116.5 ± 19.1	5.5	11.6	N/R	1.1 ± 1.2	816 ± 81	0.1	MYI
18-S8	2018-8-24	84.4°N, 156.1°W	123.5 ± 6.4	4.1	8.8	N/R	1.1 ± 1.0	809 ± 131	0.0	MYI

Note. N/R = no record.

Data Availability Statement

The field observation data are available at the website (https://doi.org/10.5281/zenodo.3779867).

Acknowledgments
This research was supported by the National Major Research High Resolution Sea Ice Model Development Program of China (2018YFA0605903), the National Natural Science Foundation of China (51639003, 41906198, and 41922045), the National Postdoctoral Program for Innovative Talents (BX20190051), the Academy of Finland (317999 and 325363), and the European Union's Horizon 2020 research and innovation program (727890–INTAROS). We thank R. Lei, W. Huang, H. Han, X. Cao, and the crews of the R/V Xuelong for their assistance with the fieldwork. The anonymous reviewers are also acknowledged for their constructive comments that highly improved the manuscript.

References

Arctic Monitoring and Assessment Programme (2011). *Snow, Water, Ice and Permafrost in the Arctic (SWIPA): Climate change and the cryosphere*. Oslo, Norway: Arctic Monitoring and Assessment Programme (AMAP).

Arctic Council (2009). Arctic marine shipping assessment report.

Assur, A. (1960). *Composition of sea ice and its tensile strength*. Wilmette, IL: U.S. Army Snow Ice and Permafrost Research Establishment.

Bitz, C. M., & Lipscomb, W. H. (1999). An energy-conserving thermodynamic model of sea ice. *Journal of Geophysical Research*, *104*(C7), 15,669–15,677. https://doi.org/10.1029/1999JC900100

Boisvert, L. N., & Stroeve, J. C. (2015). The Arctic is becoming warmer and wetter as revealed by the Atmospheric Infrared Sounder. *Geophysical Research Letters*, *42*, 4439–4446. https://doi.org/10.1002/2015GL063775

Carnat, G., Papakyriakou, T., Geilfus, N. X., Brabant, F., Delille, B., Vancoppenolle, M., et al. (2013). Investigations on physical and textural properties of Arctic first-year sea ice in the Amundsen gulf, Canada, November 2007–June 2008 (IPY-CFL system study). *Journal of Glaciology*, *59*(217), 819–837. https://doi.org/10.3189/2013JoG12J148

Cheng, B., Launianen, J., & Vihma, T. (2003). Modelling of superimposed ice formation and subsurface melting in the Baltic Sea. *Geophysica*, *39*(1–2), 31–50.

Cox, G. F. N., & Weeks, W. F. (1974). Salinity variations in sea ice. *Journal of Glaciology*, *13*(67), 109–120. https://doi.org/10.3189/s0022143000023418

Cox, G. F. N., & Weeks, W. F. (1983). Equations for determining the gas and brine volumes in sea ice samples. *Journal of Glaciology*, *29*(102), 306–316. https://doi.org/10.1017/S0022143000008364

Crabeck, O., Galley, R., Delille, B., Else, B., Geilfus, N. X., Lemes, M., et al. (2016). Imaging air volume fraction in sea ice using non-destructive X-ray tomography. *The Cryosphere*, *10*(3), 1125–1145. https://doi.org/10.5194/tc-10-1125-2016

Eicken, H., Bluhm, B. A., Collins, R. E., Gradinger, R. R., Haas, C., Ingham, M., et al. (2014). Field techniques in sea-ice research. In H. Shen (Ed.), *Cold regions science and marine technology in Encyclopedia of Life Support Systems (EOLSS)* (pp. 1–20). France: EOLSS Publishers.

Eicken, H., Krouse, H. R., Kadko, D., & Perovich, D. K. (2002). Tracer studies of pathways and rates of meltwater transport through Arctic summer sea ice. *Journal of Geophysical Research*, *107*(C10), 8046. https://doi.org/10.1029/2000JC000583

Eicken, H., & Lange, M. A. (1989). Development and properties of sea ice in the coastal regime of the southeastern Weddell Sea. *Journal of Geophysical Research*, *94*(C6), 8193–8206. https://doi.org/10.1029/JC094iC06p08193

Eicken, H., Lensu, M., Leppäranta, M., Tucker, W. B. III, Gow, A. J., & Salmela, O. (1995). Thickness, structure, and properties of level summer multiyear ice in the Eurasian sector of the Arctic Ocean. *Journal of Geophysical Research*, *100*(C11), 22,697–22,710. https://doi.org/10.1029/95JC02188

Feltham, D. L., Untersteiner, N., Wettlaufer, J. S., & Worster, M. G. (2006). Sea ice is a mushy layer. *Geophysical Research Letters*, *33*, L14501. https://doi.org/10.1029/2006GL026290

Forsström, S., Gerland, S., & Pedersen, C. A. (2011). Thickness and density of snow-covered sea ice and hydrostatic equilibrium assumption from in situ measurements in Fram Strait, the Barents Sea and the Svalbard coast. *Annals of Glaciology*, *52*(57), 261–270. https://doi.org/10.3189/172756411795931598

Frantz, C. M., Light, B., Farley, S. M., Carpenter, S., Lieblappen, R., Courville, Z., et al. (2019). Physical and optical characteristics of heavily melted "rotten" Arctic sea ice. *The Cryosphere*, *13*(3), 775–793. https://doi.org/10.5194/tc-13-775-2019

Garcia-Eidell, C., Comiso, J. C., Dinnat, E., & Brucker, L. (2017). Satellite observed salinity distributions at high latitudes in the northern hemisphere: A comparison of four products. *Journal of Geophysical Research: Oceans*, *122*, 7717–7736. https://doi.org/10.1002/2017JC013184

Gascard, J. C., Zhang, J., & Rafizadeh, M. (2019). Rapid decline of Arctic sea ice volume: Causes and consequences. *The Cryosphere Discussion*, 1–29. https://doi.org/10.5194/tc-2019-2

Golden, K. M., Ackley, S. F., & Lytle, V. I. (1998). The percolation phase transition in sea ice. *Science*, *282*(5397), 2238–2241. https://doi.org/10.1126/science.282.5397.2238

Golden, K. M., Eicken, H., Heaton, A. L., Miner, J., Pringle, D. J., & Zhu, J. (2007). Thermal evolution of permeability and microstructure in sea ice. *Geophysical Research Letters*, *34*, L16501. https://doi.org/10.1029/2007GL030447

Gosselin, M., Levasseur, M., Wheeler, P. A., Horner, R. A., & Boot, B. C. (1997). New measurements of phytoplankton and ice algal production in the Arctic Ocean. *Deep Sea Research Part II Topical Studies in Oceanography*, *44*(8), 1623–1644. https://doi.org/10.1016/S0967-0645(97)00054-4

Granskog, M. A., Rösel, A., Dodd, P. A., Divine, D. V., Gerland, S., Martma, T., & Leng, M. J. (2017). Snow contribution to first-year and second year Arctic sea ice mass balance north of Svalbard. *Journal of Geophysical Research: Oceans*, *122*, 2539–2549. https://doi.org/10.1002/2016JC012398

Huang, W., Lei, R., Han, H., & Li, Z. (2016). Physical structures and interior melt of the central Arctic sea ice/snow in summer 2012. *Cold Regions Science and Technology*, *124*, 127–137. https://doi.org/10.1016/j.coldregions.2016.01.005

Huang, W., Lei, R., Ilkka, M., Li, Q., Wang, Y., & Li, Z. (2013). The physical structures of snow and sea ice in the Arctic section of 150°–180°W during the summer of 2010. *Acta Oceanologica Sinica*, *32*(5), 57–67. https://doi.org/10.1007/s13131-013-0314-4

Hunke, E. C., & Lipscomb, W. H. (2008). *CICE: The Los Alamos sea ice model documentation and software user's manual version 4.0 LA-CC-06-012*. Los Alamos, NM: Los Alamos National Laboratory.

Hunke, E. C., Notz, D., Turner, A. K., & Vancoppenolle, M. (2011). The multiphase physics of sea ice: A review for model developers. *The Cryosphere*, *5*(4), 989–1009. https://doi.org/10.5194/tc-5-989-2011

Hutchings, J. K., Heil, P., Lecomte, O., Stevens, R., Steer, A., & Lieser, J. L. (2015). Comparing methods of measuring sea-ice density in the East Antarctic. *Annals of Glaciology*, *56*(69), 77–82. https://doi.org/10.3189/2015AoG69A814

Jeffries, M. O., Krouse, H. R., Hurst-Cushing, B., & Maksym, T. (2001). Snow-ice accretion and snow-cover depletion on Antarctic first-year sea-ice floes. *Annals of Glaciology*, *33*(1), 51–60. https://doi.org/10.3189/172756401781818266

Lange, M. A., & Eicken, H. (1991). Textural characteristics of sea ice and the major mechanisms of ice growth in the Weddell Sea. *Annals of Glaciology*, *15*(69), 210–215. https://doi.org/10.3189/1991aog15-1-210-215

Leppäranta, M., & Manninen, T. (1988). *The brine and gas content of sea ice with attention to low salinities and high temperatures*. Helsinki: Finnish Institute of Marine Research.
Light, B., Maykut, G. A., & Grenfell, T. C. (2003). Effects of temperature on the microstructure of first-year Arctic sea ice. *Journal of Geophysical Research*, *108*(C2), 3051. https://doi.org/10.1029/2001JC000887
Light, B., Maykut, G. A., & Grenfell, T. C. (2004). A temperature-dependent, structural-optical model of first-year sea ice. *Journal of Geophysical Research*, *109*, C06013. https://doi.org/10.1029/2003JC002164
Lindsay, R., & Schweiger, A. (2015). Arctic Sea ice thickness loss determined using subsurface, aircraft, and satellite observations. *The Cryosphere*, *9*(1), 269–283. https://doi.org/10.5194/tc-9-269-2015
Markus, T., Stroeve, J. C., & Miller, J. (2009). Recent changes in Arctic Sea ice melt onset, freezeup, and melt season length. *Journal of Geophysical Research*, *114*, C12024. https://doi.org/10.1029/2009JC005436
Maslanik, J. A., Fowler, C., Stroeve, J., Drobot, S., Zwally, J., Yi, D., & Emery, W. (2007). A younger, thinner Arctic ice cover: Increased potential for rapid, extensive sea-ice loss. *Geophysical Research Letters*, *34*, L24501. https://doi.org/10.1029/2007GL032043
Meese, D. A. (1989). *The chemical and structural properties of sea ice in the southern Beaufort Sea*. Hanover: Cold Regions Research Engineering Laboratory.
Meier, W. N., Hovelsrud, G. K., van Oort, B. E. H., Key, J. R., Kovacs, K. M., Michel, C., et al. (2014). Arctic sea ice in transformation: A review of recent observed changes and impacts on biology and human activity. *Reviews of Geophysics*, *52*, 185–217. https://doi.org/10.1002/2013RG000431
Merkouriadi, I., Liston, G. E., Graham, R. M., & Granskog, M. A. (2020). Quantifying the potential for snow-ice formation in the Arctic Ocean. *Geophysical Research Letters*, *47*, e2019GL085020. https://doi.org/10.1029/2019GL085020
Nakawo, M. (1983). Measurements on air porosity of sea ice. *Annals of Glaciology*, *4*, 204–208. https://doi.org/10.1017/S0260305500005486
Nakawo, M., & Sinha, N. K. (1981). Growth rate and salinity profile of first-year sea ice in the high Arctic. *Journal of Glaciology*, *27*(96), 315–330. https://doi.org/10.1017/S0022143000015409
Notz, D., Wettlaufer, J. S., & Worster, M. G. (2005). A non-destructive method for measuring the salinity and solid fraction of growing sea ice in situ. *Journal of Glaciology*, *51*(172), 159–166. https://doi.org/10.3189/172756505781829548
Notz, D., & Worster, M. G. (2009). Desalination processes of sea ice revisited. *Journal of Geophysical Research*, *114*, C05006. https://doi.org/10.1029/2008JC004885
Overgaard, S., Wadhams, P., & Leppäranta, M. (1983). Ice properties in the Greenland and Barents Seas during summer. *Journal of Glaciology*, *29*(101), 142–164. https://doi.org/10.1017/S0022143000005219
Perovich, D. K., & Elder, B. C. (2001). Temporal evolution of Arctic sea-ice temperature. *Annals of Glaciology*, *33*, 207–211. https://doi.org/10.3189/172756401781818158
Perovich, D. K., & Gow, A. J. (1996). A quantitative description of sea ice inclusions. *Journal of Geophysical Research*, *101*(C8), 18,327–18,343. https://doi.org/10.1029/96JC01688
Perovich, D. K., & Grenfell, T. C. (1981). Laboratory studies of the optical properties of young sea ice. *Journal of Glaciology*, *27*(96), 331–346. https://doi.org/10.1017/S0022143000015410
Perovich, D. K., Grenfell, T. C., Light, B., Elder, B. C., Harbeck, J., Polashenski, C., et al. (2009). Transpolar observations of the morphological properties of Arctic sea ice. *Journal of Geophysical Research*, *114*, C00A04. https://doi.org/10.1029/2008JC004892
Pustogvar, A., & Kulyakhtin, V. (2016). Sea ice density measurements: Methods and uncertainties. *Cold Regions Science and Technology*, *131*, 46–52. https://doi.org/10.1016/j.coldregions.2016.09.001
Razali, N. M., & Wah, Y. B. (2011). Power comparisons of Shapiro-Wilk, Kolmogorov-Smirnov, Lilliefors and Anderson-Darling tests. *Journal of Statistical Modeling and Analytics*, *2*(1), 21–33.
Riihelä, A., Manninen, T., & Laine, V. (2013). Observed changes in the albedo of the Arctic sea-ice zone for the period 1982–2009. *Nature Climate Change*, *3*(10), 895–898. https://doi.org/10.1038/NCLIMATE1963
Schwarzacher, W. (1959). Pack-ice studies in the Arctic Ocean. *Journal of Geophysical Research*, *64*(12), 2357–2367. https://doi.org/10.1029/JZ064i012p02357
Screen, J. A., & Simmonds, I. (2010). The central role of diminishing sea ice in recent Arctic temperature amplification. *Nature*, *464*(7293), 1334–1337. https://doi.org/10.1038/nature09051
Smith, L. C., & Stephenson, S. R. (2013). New Trans-Arctic shipping routes navigable by midcentury. *Proceedings of the National Academy of Sciences*, *110*(13), E1191–E1195. https://doi.org/10.1073/pnas.1214212110
Sturm, M., & Massom, R. (2010). Snow on sea ice. In D. N. Thomas, & G. S. Dieckmann (Eds.), *Sea Ice* (Second ed. pp. 153–204). Hoboken: Wiley-Blackwell.
Timco, G. W., & Frederking, R. M. W. (1996). A review of sea ice density. *Cold Regions Science and Technology*, *24*(1), 1–6. https://doi.org/10.1016/0165-232X(95)00007-X
Timco, G. W., & Weeks, W. F. (2010). A review of the engineering properties of sea ice. *Cold Regions Science and Technology*, *60*(2), 107–129. https://doi.org/10.1016/j.coldregions.2009.10.003
Tucker, W. B. III, Gow, A. J., Meese, D. A., Bosworth, H. W., & Reimnitz, E. (1999). Physical characteristics of summer sea ice across the Arctic Ocean. *Journal of Geophysical Research*, *104*(C1), 1489–1504. https://doi.org/10.1029/98JC02607
Tucker, W. B. III, Gow, A. J., & Weeks, W. F. (1987). Physical properties of summer sea ice in the Fram Strait. *Journal of Geophysical Research*, *92*(C7), 6787–6803. https://doi.org/10.1029/JC092iC07p06787
Ukita, J., Kawamura, T., Tanaka, N., Toyota, T., & Wakatsuchi, M. (2000). Physical and stable isotopic properties and growth processes of sea ice collected in the southern Sea of Okhotsk. *Journal of Geophysical Research*, *105*(C9), 22,083–22,093. https://doi.org/10.1029/1999JC000013
Vancoppenolle, M., Fichefet, T., & Bitz, C. M. (2006). Modeling the salinity profile of undeformed Arctic sea ice. *Geophysical Research Letters*, *33*, L21501. https://doi.org/10.1029/2006GL028342
Vihma, T. (2014). Effects of Arctic sea ice decline on weather and climate: A review. *Surveys in Geophysics*, *35*(5), 1175–1214. https://doi.org/10.1007/s10712-014-9284-0
Vihma, T., Pirazzini, R., Fer, I., Renfrew, I. A., Sedlar, J., Tjernström, M., et al. (2014). Advances in understanding and parameterization of small-scale physical processes in the marine Arctic climate system: A review. *Atmospheric Chemistry and Physics*, *14*(17), 9403–9450. https://doi.org/10.5194/acp-14-9403-2014
Wang, Q., Li, Z., Lei, R., Lu, P., & Han, H. (2018). Estimation of the uniaxial compressive strength of Arctic sea ice during melt season. *Cold Regions Science and Technology*, *151*, 9–18. https://doi.org/10.1016/j.coldregions.2018.03.002
Yen, Y. (1981). *Review of thermal properties of snow, ice and sea ice*. Hanover: Cold Regions Research Engineering Laboratory.